Quantized thermoelectric Hall plateau in the quantum limit of graphite as a nodal-line semimetal

Andhika Kiswandhi,* Tomotaka Ochi, Toshihiro Taen, Mitsuyuki Sato, Kazuhito Uchida, and Toshihito Osada†
Institute for Solid State Physics, University of Tokyo, 5-1-5 Kashiwanoha, Kashiwa, Chiba 277-8581, Japan

(Received 8 November 2022; revised 24 March 2023; accepted 24 April 2023; published 4 May 2023)

We performed thermoelectric Hall conductivity α_{xy} measurements on single-crystal graphite in the quantum limit up to 13 T. Both electrical and thermoelectric transport measurements were performed on the same crystal to extract pure α_{xy}, avoiding any sample quality dependence. The α_{xy} converges to a plateau in the quantum limit with a linear dependence on temperature. This behavior is analogous to the quantized thermoelectric Hall effect (QTHE) observed in three-dimensional Dirac/Weyl nodal-point semimetals, and experimentally confirms a theoretical proposal on the QTHE in semimetals with nodal lines as in graphite.

DOI: 10.1103/PhysRevB.107.195106

I. INTRODUCTION

Thermoelectric effects in three-dimensional (3D) Dirac/Weyl semimetals (DWSM) under a high magnetic field have been theoretically investigated in recent years. Under a dissipationless condition, the thermoelectric Hall conductivity α_{xy} was found to converge to a plateau, proportional to temperature (T), but independent of carrier density and magnetic field strength (B) upon entering the quantum limit (QL) [1]. This phenomenon is known as the quantized thermoelectric Hall effect (QTHE). Here, α_{xy} is an off-diagonal element of the thermoelectric conductivity tensor $\overleftrightarrow{\alpha}$ defined by $\mathbf{j} = \overleftrightarrow{\sigma}\mathbf{E} + \overleftrightarrow{\alpha}(-\nabla T)$, where $\mathbf{j}$, $\mathbf{E}$, $\overleftrightarrow{\sigma}$, and $-\nabla T$ are the current density, electric field, electrical conductivity tensor, and temperature gradient, respectively. The Seebeck coefficient S_{xx} is the diagonal element of the thermopower tensor $\overleftrightarrow{S} = \overleftrightarrow{\sigma}^{-1}\overleftrightarrow{\alpha}$. QTHE originates from the gapless chiral $N = 0$ Landau levels (LLs) in 3D DWSM with an energy-independent density of states (DOS), which distinguish them from single-band metals. The QTHE together with the gapless chiral LLs imply S_{xx} grows linearly with B without an upper limit [2]. Such properties make 3D DWSM attractive for realizing a tunable, high-performance thermoelectricity-based power generation at low temperatures, where other materials are impractical. Experimentally, the B-linear increase of S_{xx} at QL has been reported in a 3D Dirac semimetal with a small spin-orbit gap $Pb_{1-x}Sn_xSe$ and Weyl semimetal TaP [3,4]. A feature consistent with the α_{xy} plateau has been observed in TaP and the 3D Dirac semimetal $ZrTe_5$ [4,5]. In $ZrTe_5$, although S_{xx} appears to not strictly follow the B-linear behavior, attributed to a possible variation in the carrier balance, α_{xy} remains approaching a constant value at high B, in agreement with the theory that α_{xy} is independent of carrier balance. Therefore, a quantized α_{xy} plateau can be taken as a signature of a 3D DWSM [4,5].

However, QTHE is not necessarily unique to 3D Dirac/Weyl nodal-point semimetals. Our simulation using a straight Dirac nodal-line semimetal model, equivalent to a stack of 2D Dirac fermion layers, yields a similar energy-independent DOS for its lowest LL. Here, we denote LLs of DWSM and nodal-line semimetal by N, while those of graphite by N'. The LL structure of the nodal-line semimetal [Fig. 1(c)] shows a nonchiral $N = 0$ LL, but around the Fermi level it shows a similar configuration as the chiral $N = 0$ LLs of a pair of Dirac/Weyl cones in a 3D DWSM shown in Fig. 1(a) [6]. The calculated B dependence of α_{xy} in the dissipationless case [Fig. 1(d)] shows qualitatively the same plateau behavior at the QL as that predicted for DWSMs in Ref. [1] shown schematically in Fig. 1(b).

Such a straight nodal-line semimetal configuration can be found in graphite. The LL subband dispersion for graphite [Fig. 1(e)], calculated using the Slonczewski-Weiss-McClure model [7,8], with trigonal warping ignored shows the conduction and valence bands touch along the H-K-H edge in the $\mathbf{k}$ space, forming a straight nodal line [9]. This configuration is very similar to that of the straight nodal-line semimetal in Fig. 1(c), except that there are two lowest LLs with $N' = 0, -1$, corresponding to the doubly degenerate lowest LL of the bilayer graphene stacking unit. Therefore, the QTHE can be expected in graphite at the quasi-QL where the chemical potential μ crosses only the $N' = 0, -1$ subbands as shown in Fig. 1(f) [6].

The electrical resistivities (longitudinal resistivity ρ_{xx} and Hall resistivity ρ_{xy}, where $\overleftrightarrow{\rho} = \overleftrightarrow{\sigma}^{-1}$) and the Seebeck coefficient S_{xx} of graphite up to the quasi-QL have been extensively studied [10–12], with their Nernst coefficient S_{xy} under a magnetic field explored only recently [13,14]. However, partial measurements on separate crystals are not ideal for $\alpha_{xy}(B)$ since ρ_{xx}, ρ_{xy}, S_{xx}, and S_{xy} may vary with different crystals. In this paper, we experimentally confirm QTHE in graphite by performing transport and thermoelectric measurements on the same graphite single crystal.

II. EXPERIMENTAL

A bulk graphite sample with a dimension of $37 \times 0.8 \times 0.065\ \mathrm{mm}^3$ was prepared by cleaving a Kish graphite crystal using an adhesive tape. On the clean surface, six gold

*kiswandhi@issp.u-tokyo.ac.jp
†osada@issp.u-tokyo.ac.jp

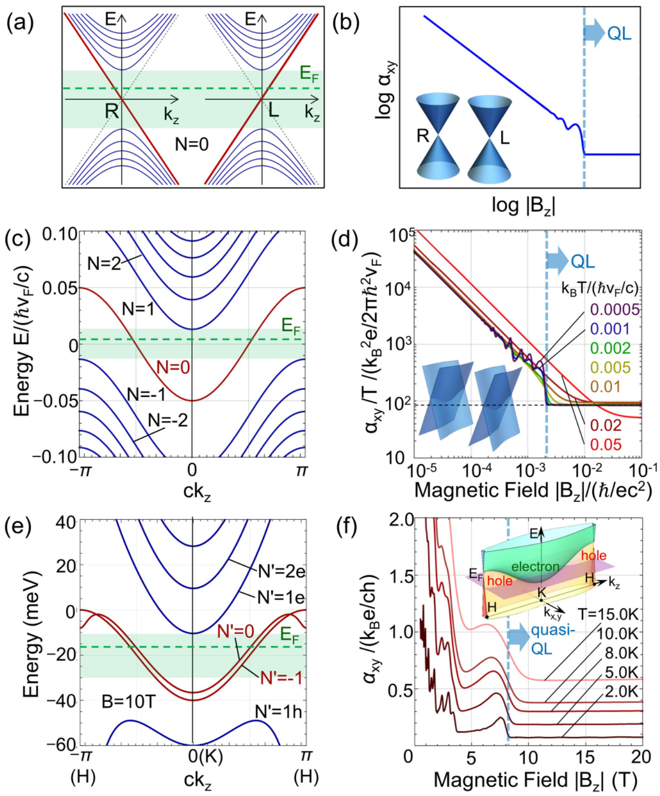

FIG. 1. Landau subband dispersion and B dependence of α_{xy} for (a) and (b) Dirac/Weyl nodal-point semimetals [(b) is a schematic, after Ref. [1]], (c) and (d) a semimetal with straight Dirac nodal lines, and (e) and (f) bulk graphite (after Ref. [6]). Here, v_F, t_c, and c are the in-plane Fermi velocity, interlayer transfer integral, and interlayer spacing of multilayer semimetals with straight Dirac nodal lines, respectively. The insets of (b), (d), and (f) illustrate the band dispersion of the Dirac/Weyl nodal-point semimetal, band dispersion of the semimetal with straight Dirac nodal lines, and band dispersion of graphite, respectively. (c) was calculated using $2t_c/(\hbar v_F/c) = 0.05$ and $|B_z|/(\hbar/ec^2) = 0.002$, and (d) was calculated using $(n-p)c^3 = 1 \times 10^{-4}$.

wires were attached in a standard Hall configuration. The sample was placed on a thermoelectric measurement platform (Fig. 2), on which electrical transport measurements were also performed. For the thermoelectric measurements, two chromel-constantan thermocouples were attached to the sample. All measurements were performed with the dc mode under a magnetic field up to 13 T parallel to the stacking direction. To eliminate mixing between $\rho_{xx}(S_{xx})$ and $\rho_{xy}(S_{xy})$ signals that may arise due to contact misalignment, signals were collected in both positive and negative field directions, then standard symmetrization and antisymmetrization procedures were used. The reported S_{xx} values are relative to the gold wire electrodes with $S_{\mathrm{Au}} \approx 1$ µV/K up to 30 T [15,16], so it should be understood not to deduce the carrier type using S_{xx} directly. (See also the Supplemental Material for details [17].)

III. RESULTS AND DISCUSSION

Figure 3 summarizes all of the measured quantities in this work. As a reference, we consider the electrical current flow

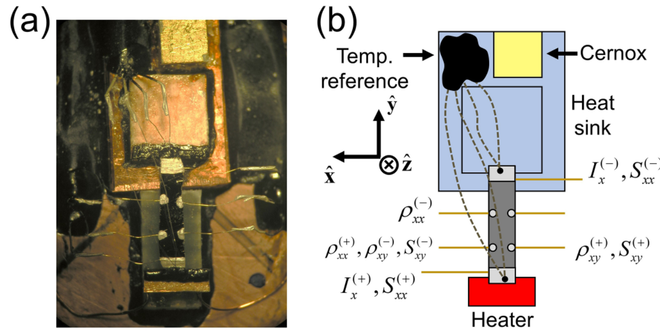

FIG. 2. (a) Photograph of the experimental setup and (b) schematic of the experimental setup corresponding to (a). The sample is attached between a heater and copper heat sink. Two thermocouples (dashed line) measure the temperatures on the heater side and heat sink side of the sample. The thermocouples were thermally referenced to the heat sink adjacent to a Cernox thermometer. The symbols denote electrode connections to the sample, where (+) and (−) superscripts denote positive and negative electrodes, respectively.

and temperature gradient directions to be $\mathbf{I} \parallel -\nabla T$ and $\mathbf{B} \parallel \hat{\mathbf{z}}$. To standardize notation, we report the transverse coefficients as ρ_{xy} and S_{xy} unless otherwise noted. Magnetic field dependences of ρ_{xx} and ρ_{xy} taken at several fixed temperatures are shown in Figs. 3(a) and 3(b), respectively [note $-\rho_{xy}$ in Fig. 3(b)]. Typical Shubnikov–de Haas (SdH) oscillations are clearly seen with the last oscillation appearing at $B \approx 7.5$ T. As B increases, the SdH oscillation amplitude increases, such that the last peak anomalously crosses zero. The zero crossing ρ_{xy} has been observed in some experiments, and appears to be sample dependent with some reports show no sign change at high field [12,18–20]. The sign change may occur in the Shubnikov–de Haas regime due to the changing balance between the number of electrons and holes, and more recently shown to be related to possible disorder upon doping. Our Kish graphite sample shows a sign change around $B = 6.8$ T, similar to the undoped sample in Refs. [18,20]. Our interests here are the facts that both ρ_{xx} and ρ_{xy} appear to be only weakly dependent on the temperatures within the range considered and that $|\rho_{xy}| \ll |\rho_{xx}|$ throughout the field sweep.

From these data, the conductivities σ_{xx} and σ_{xy} can be obtained by inverting the resistivity matrix, or explicitly, $\sigma_{xx} = \rho_{xx}/(\rho_{xx}^2 + \rho_{xy}^2)$ and $\sigma_{xy} = -\rho_{xy}/(\rho_{xx}^2 + \rho_{xy}^2)$. Since $|\rho_{xy}| \ll |\rho_{xx}|$ one sees immediately that $|\sigma_{xy}| \ll |\sigma_{xx}|$. This is in contrast to the dissipationless limit condition $\sigma_{xx} = 0$, and is always true for graphite [19,21]. For this reason, the difference between electron and hole densities cannot be obtained by using the usual Hall coefficient $R_H \to 1/e(n-p)$, where n and p are the electron and the hole density, respectively [19]. As an alternative, we used the SdH oscillations to obtain $n - p$. A Fourier transform of $d^2\rho_{xx}/dB^2$ yields two dominant components with frequencies of 4.72 and 6.42 T. These frequencies correspond to carrier pockets located near the H and K points, respectively, in agreement with known results [11,22]. Taking into account the geometry and the multiplicity of the pockets in the Brillouin zone, we found $|n-p| \approx 6 \times 10^{17}/\mathrm{cm}^3$, about half of the value used in our calculations [6]. (See also

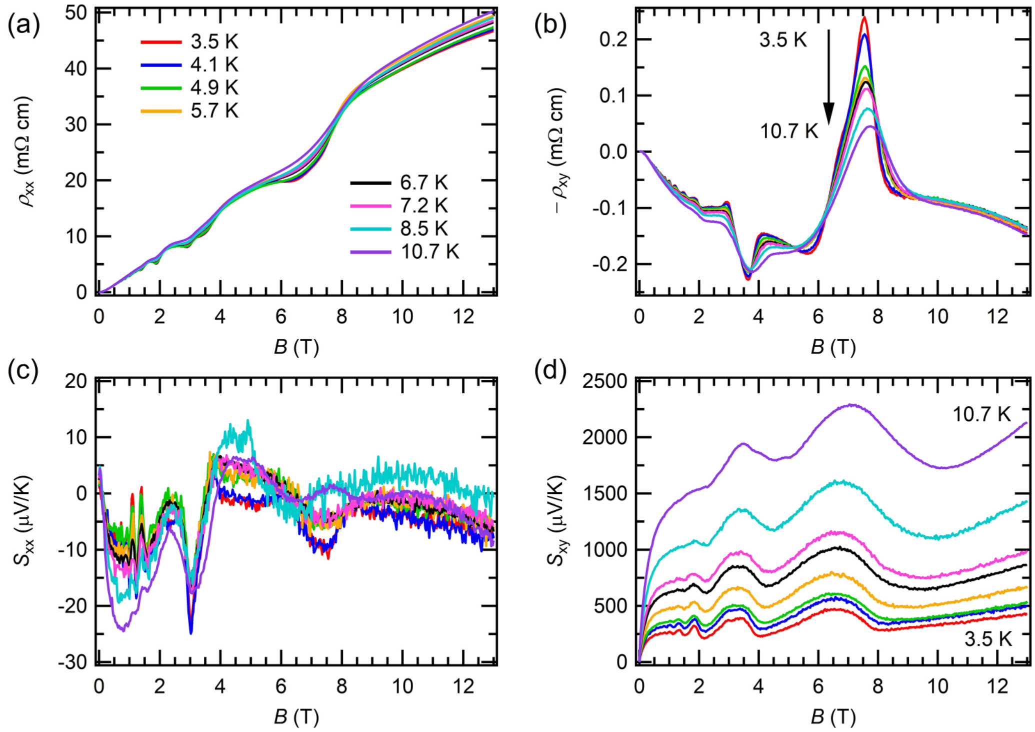

FIG. 3. Magnetic field dependence at several fixed temperatures for (a) resistivity ρ_{xx}, (b) Hall resistivity (note: $-\rho_{xy}$), (c) Seebeck coefficient S_{xx}, and (d) Nernst coefficient S_{xy}.

the Supplemental Material for the temperature dependence of the SdH frequencies [17].)

Next, we look into the thermoelectric coefficients S_{xx} and S_{xy} shown in Figs. 3(c) and 3(d), respectively. One again sees a typical SdH-type oscillatory behavior. In contrast to the transport coefficients where $|\rho_{xy}| \ll |\rho_{xx}|$, here S_{xx} is dwarfed by S_{xy} at all temperatures. Note that while S_{xx} is not strongly dependent on T, S_{xy} is very well resolved with T due to its strong response at low B. The curves behave as $S_{xy} \propto T$ for $T \leqslant 5.7$ K throughout the magnetic field range. At $B \geqslant 8$ T, S_{xy} gains a B-linear behavior. This implies $S_{xy} \propto (BT)$ in the QL regime, similar to the behavior reported in Refs. [13,14]. At higher temperatures, the curves deviate from the $S_{xy} \propto T$ tendency, but generally remain proportional to B. (See also the Supplemental Material for the B and T dependences of S_{xy} [17].)

Having seen each of ρ_{xx}, ρ_{xy}, S_{xx}, and S_{xy} separately, we now turn our attention to α_{xy}. Thermoelectric Hall conductivity α_{xy} relates all the quantities above, and is written explicitly as

$$\alpha_{xy} = \frac{1}{\rho_{xx}^2 + \rho_{xy}^2}(\rho_{xx}S_{xy} - \rho_{xy}S_{xx}). \tag{1}$$

The term $\rho_{xy}S_{xx}$ is overwhelmed by $\rho_{xx}S_{xy}$ by 3–4 orders of magnitude. Assuming a Seebeck coefficient of a gold wire of $S_{\mathrm{Au}} \sim 1$ μV/K, its contribution will only change the overall α_{xy} by about 0.01%, so neglecting its contribution in α_{xy} can be justified, although not necessarily negligible when considering only S_{xx}.

Considering that the coefficients other than S_{xy} are not modified significantly by temperature, it is expected that the T-linear dependence of S_{xy} is reflected in α_{xy}. Figure 4(a) shows α_{xy}/T calculated from the experimental data using Eq. (1). For convenience, here we plot the dimensionless $\alpha_{xy}/(k_{\mathrm{B}}e/ch)$, where k_{B} is the Boltzmann constant, $e(>0)$ is the elementary charge, c is the c-axis lattice constant ($c/2 = 0.337$ nm), and h is the Planck constant. The general behavior follows closely the predicted behavior for graphite illustrated in Fig. 1(f). At low fields the curves first show a monotonic decrease with $\alpha_{xy} \propto B^{-1}$ dependence as shown in the inset of Fig. 4(a), consistent with the predicted behavior for the straight nodal-line semimetal shown in Fig. 1(d). Up to 5.7 K, the curves follow an overall $\alpha_{xy} \propto T/B$ behavior. As B is increased even further beyond the last SdH oscillation, the system enters the quasi-QL.

Upon entering the quasi-QL region α_{xy} changes slope and tends to a value independent of B. This plateau extends from the last SdH peak to the maximum field at each temperature, which is expected to be a manifestation of the QTHE. To clearly show its T dependence, α_{xy} points taken at several fixed B are shown in Fig. 4(b). In a general case of multilayer semimetals with straight nodal lines, we have previously found that the plateau value is given approximately by the following, including spin and valley degeneracy [6],

$$\alpha_{xy}/(k_{\mathrm{B}}e/ch) = \frac{2\pi k_{\mathrm{B}}T}{3t_c}. \tag{2}$$

Here, t_c is the interlayer transfer integral. For graphite, Eq. (2) gains an additional factor of two coming from the doubly degenerate lowest LL subbands $N' = 0, -1$. The value of t_c can be estimated from the width of the B-independent $N' = -1$ subband given by $4t_c \approx 40$ meV, and the same value was assumed for the $N' = 0$ subband. With this value, one obtains $\alpha_{xy}/(k_{\mathrm{B}}e/ch) \approx 0.036\ (\mathrm{K}^{-1}) \times T$. The plateaus followed this

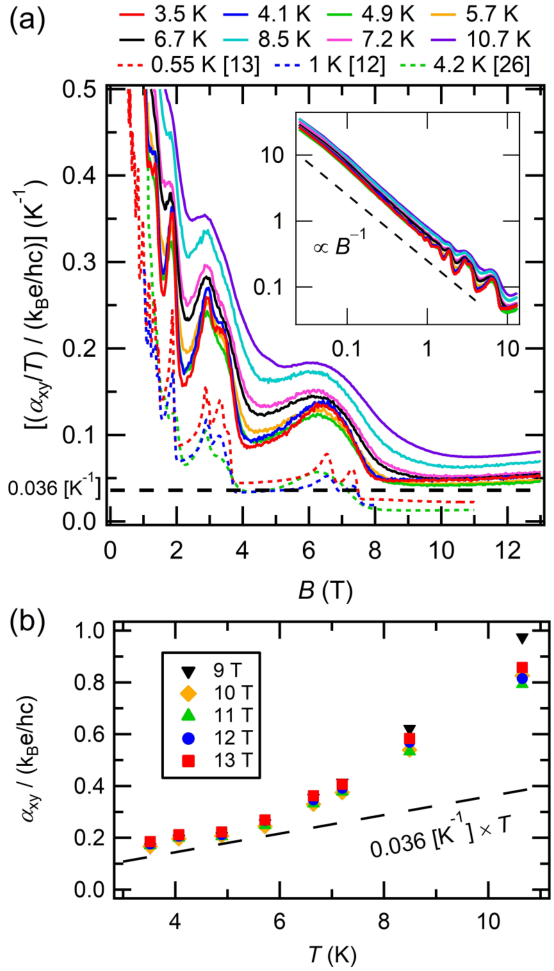

FIG. 4. (a) Magnetic field dependence of thermoelectric Hall conductivity $(\alpha_{xy}/T)/(k_Be/ch)$ obtained from the transport and thermoelectric measurements showing behavior consistent with Ref. [6]. The curves overlap with each other at $T \leqslant 5.7$ K and are quantized to a value that depends only on t_c. Dashed lines are α_{xy} calculated using transport data taken from Refs. [12,13,26] combined with S_{xy} data from Ref. [13]. The inset shows the low-field region $\alpha_{xy} \propto B^{-1}$ behavior consistent with the behavior shown in Fig. 1(b) for a semimetal with straight nodal lines. (b) Temperature dependence of α_{xy} at several fixed magnetic fields, showing a T-linear dependence as predicted in Eq. (2).

behavior not only qualitatively, but quantitatively as well for $T \leqslant 5.7$ K. This fact strongly suggests that the observed behavior results from the QTHE predicted in graphite. Above 5.7 K the slope becomes steeper, indicating a deviation from $\alpha_{xy} \propto T$ although the plateau survives. This is the same deviation seen in S_{xy}. Theoretically, the T-linear behavior is expected at the low-temperature region defined by $k_BT \ll t_c$, which corresponds to $T \ll 110$ K for graphite. However, it should be noted that this is based on transport in the clean limit without phonon scattering. In reality, the phonon drag effect enhances both S_{xx} and S_{xy} [23,24]. Our observation of $\alpha_{xy} \propto T$ occurs at $T \ll 15$ K, where a peak in S_{xx} can be observed. This temperature is similar to the reported S_{xx} peak temperature by another group [25], and so is likely a consequence of the phonon drag effect. (See Supplemental Material for the temperature dependence of S_{xx} and measurement results at extended temperatures [17].)

Here, we compare our result with data published by other groups. We took the transport data for 0.55, 1.1, and 4.2 K from Refs. [12,13,26] and S_{xy} data with the closest matching temperatures from Ref. [13]. As shown in Fig. 4(a), α_{xy} calculated using these data show a plateau at QL with the correct order of magnitude, but with values lower than predicted by Eq. (2). However, differences in the reported magnitudes of $\rho_{xx}(B)$ make it difficult to compare the resulting α_{xy}. As far as we know similar complete measurements on one sample have been performed so far only by Zhu *et al.* on their sample labeled “HOPG sample 2” [13]. For this sample, assuming that ρ_{xx} does not vary much with temperature, we approximated $\alpha_{xy}/(k_Be/ch) \approx 0.023$ (K^{-1}) $\times T$. However, since $\alpha_{xy} \approx S_{xy}/\rho_{xx}$ and $d\rho_{xx}/dT > 0$, their T dependence of α_{xy} likely follows a gentler slope than the estimate above.

Now, we address the slight deviation from the α_{xy} plateau predicted by Eq. (2). Using this equation, any deviation from the plateau can only be introduced via t_c, with others being some fundamental constants. In the case of graphite, however, it is not perfectly accurate to employ Eq. (2) because the Fermi velocity (related to the subband width) of the $N' = 0$ LL is slightly different from that of the $N' = -1$ LL. This difference introduces a deviation of less than 1% compared with Eq. (2) at $T = 5$ K. Additionally, whereas the Fermi velocity of the $N' = -1$ subband has no B dependence, the $N' = 0$ has a weak B dependence [27,28]. The B dependence of the $N' = 0$ LL subband is such that its Fermi velocity decreases with increasing field, consequently α_{xy} tends to rise on average. This may be the reason why the QTHE plateau of α_{xy} deviates from 0.036 (K^{-1}) $\times$ $(k_Be/ch)T$ and show a weak B dependence.

Next, we comment on the nonappearance of the B-linear S_{xx} in graphite despite the α_{xy} plateau. For a chiral LL of 3D DWSM, the DOS is energy independent, which is responsible for the α_{xy} plateau. In the dissipationless limit $(\sigma_{xx} \to 0)$, S_{xx} is given by $S_{xx} \approx \alpha_{xy}/\sigma_{xy} = -\alpha_{xy}B_z/e(n-p)$. Therefore, the B-linear growth occurs for constant $n - p$. For graphite, the DOS is approximately energy independent, but because the system is dissipative $(\sigma_{xx} \gg \sigma_{xy})$, the S_{xx} approximation above does not apply, so the B-linear increase of S_{xx} cannot be expected. However, the α_{xy} plateau behavior survives because it corresponds to the dominant leading term of α_{xy} in the dissipative system [6].

Finally, the present model can be extended for systems having multiple straight nodal lines, given that those nodal lines are parallel to the applied magnetic field. Equation (2) implicitly already contains a factor of two, originating from the two valleys shown in the inset of Fig. 1(d). In the case of multiple straight nodal lines parallel to a magnetic field, Eq. (2) is modified to include the total number of straight nodal lines. This specific case is similar to the case of DWSM with a multiple Dirac nodes discussed in Refs. [1,2].

IV. CONCLUSION

In conclusion, we have demonstrated that graphite shows QTHE as a straight nodal-line semimetal. Although the system is dissipative, the dissipationless leading term of α_{xy} exhibiting the QTHE plateau becomes dominant. The unlimited B-linear increase of S_{xx} cannot be expected in this case, but α_{xy} remains quantized due to an energy-independent density of states, similar to 3D Dirac/Weyl nodal-point semimetals. The present result shows that quantized α_{xy} is a strong indicator of 3D DWSM, but not their exclusive property.

ACKNOWLEDGMENTS

The authors thank Prof. Sonia Haddad for valuable discussions, and Prof. Woun Kang for his technical advice on thermoelectric measurements. This work was supported by JSPS KAKENHI Grants No. JP19K14655, No. JP20H01860, and No. JP21K18594.

[1] V. Kozii, B. Skinner, and L. Fu, Phys. Rev. B **99**, 155123 (2019).
[2] B. Skinner and L. Fu, Sci. Adv. **4**, eaat2621 (2018).
[3] T. Liang, Q. Gibson, J. Xiong, M. Hirschberger, S. P. Koduvayur, R. J. Cava, and N. P. Ong, Nat. Commun. **4**, 2696 (2013).
[4] F. Han, N. Andrejevic, T. Nguyen, V. Kozii, Q. T. Nguyen, T. Hogan, Z. Ding, R. Pablo-Pedro, S. Parjan, B. Skinner, A. Alatas, E. Alp, S. Chi, J. Fernandez-Baca, S. Huang, L. Fu, and M. Li, Nat. Commun. **11**, 6167 (2020).
[5] W. Zhang, P. Wang, B. Skinner, R. Bi, V. Kozii, C.-W. Cho, R. Zhong, J. Schneeloch, D. Yu, G. Gu, L. Fu, X. Wu, and L. Zhang, Nat. Commun. **11**, 1046 (2020).
[6] T. Osada, T. Ochi, and T. Taen, J. Phys. Soc. Jpn. **91**, 063701 (2022).
[7] J. C. Slonczewski and P. R. Weiss, Phys. Rev. **109**, 272 (1958).
[8] J. W. McClure, Phys. Rev. **108**, 612 (1957).
[9] G. P. Mikitik and Y. V. Sharlai, Phys. Rev. B **73**, 235112 (2006).
[10] D. E. Soule, Phys. Rev. **112**, 698 (1958).
[11] D. E. Soule, Phys. Rev. **112**, 708 (1958).
[12] J. A. Woollam, Phys. Rev. B **3**, 1148 (1971).
[13] Z. Zhu, H. Yang, B. Fauqué, Y. Kopelevich, and K. Behnia, Nat. Phys. **6**, 26 (2010).
[14] B. Fauqué, Z. Zhu, T. Murphy, and K. Behnia, Phys. Rev. Lett. **106**, 246405 (2011).
[15] E. S. Choi, J. S. Brooks, J. S. Qualls, and Y. S. Song, Rev. Sci. Instrum. **72**, 2392 (2001).
[16] E. S. Choi, H. Kang, Y. J. Jo, and W. Kang, Rev. Sci. Instrum. **73**, 2999 (2002).
[17] See Supplemental Material at http://link.aps.org/supplemental/10.1103/PhysRevB.107.195106 for more details of the sample and the measurement methods, including the magnetic field dependence of S_{xy} and high temperature data.
[18] R. F. de Jesus, B. C. Camargo, R. R. da Silva, Y. Kopelevich, M. Behar, M. A. Gusmão, and P. Pureur, Phys. B: Condens. Matter **500**, 118 (2016).
[19] I. L. Spain, Carbon **17**, 209 (1979).
[20] S. B. Hubbard, T. J. Kershaw, A. Usher, A. K. Savchenko, and A. Shytov, Phys. Rev. B **83**, 035122 (2011).
[21] J. W. McClure and W. J. Spry, Phys. Rev. **165**, 809 (1968).
[22] J. M. Schneider, M. Orlita, M. Potemski, and D. K. Maude, Phys. Rev. Lett. **102**, 166403 (2009).
[23] K. Sugihara, H. Ohshima, K. Kawamura, and T. Tsuzuku, J. Phys. Soc. Jpn. **43**, 1664 (1977).
[24] J.-P. Jay-Gerin, Solid State Commun. **19**, 119 (1976).
[25] T. Tokumoto, E. Jobiliong, E. S. Choi, Y. Oshima, and J. S. Brooks, Solid State Commun. **129**, 599 (2004).
[26] L. W. Kreps and J. A. Woollam, Carbon **15**, 403 (1977).
[27] M. Inoue, J. Phys. Soc. Jpn. **17**, 808 (1962).
[28] K. Nakao, J. Phys. Soc. Jpn. **40**, 761 (1976).